Optical and Quantum Electronics (2023) 55:292
https://doi.org/10.1007/s11082-023-04569-3

Investigation of the electronic and optical activity of halogen-substituted 2-nitrotoulene by density functional theory

Shradha Lakhera[1] · Meenakshi Rana[1] · Kamal Devlal[1]

Received: 28 September 2022 / Accepted: 9 January 2023

Abstract
The enhancement of Nonlinear optical (NLO) activity of the 2-nitrotoulene (2NT) after the substitution of the halogens (F, Cl, Br, and I) at the para position of the benzene ring was reported in the paper. All the computational details were mentioned using density functional theory with B3LYP/6-311++G(d,p) basis set. The engagement of the electrophilic and nucleophilic regions in molecules was established using contour plots. Mulliken charge analysis and frontier molecular orbital parameters laid the high chemical reactivity of 2NT molecule after the substitution of F, Cl, Br, and I. Using time-dependent density functional theory, electronic properties were analyzed by computing absorption and emission spectra. The higher Raman intensity modes and higher absorbance intensity curve for iodine-substituted 2NT (2NT-I) highlighted the highest reactivity. The lowest band gap was reported for 2NT-I (4.02 eV) which better correlates with the charge and spectral findings. The polarizability parameters set a fair comparison between the NLO activities of the molecules. 2NT-I has the highest values of polarizability parameters among the other molecules.

Keywords Density functional theory · Nonlinear optics · 2-Nitrotoulene · Halogens · Hyperpolarizability

1 Introduction

Nitrotoulene (NT) is an aromatic compound having numerous applications in pigments, antioxidants, agricultural chemicals, and photographic chemicals (Lin et al. 2007; Felscia and Rajkumar 2018; Wen et al. 2012; Yanzhu et al. 2022). It mainly comprises a nitro group that is highly electronegative in nature and a methyl group that acts as a strong electron donor moiety (Majee et al. 2019). The inductive effect leads to the liberation of the electrons from the methyl group towards the nitro group and the charge gets transferred to the benzene ring. The free electrons thus, result in hyperconjugation, and the benzene ring

✉ Meenakshi Rana
mrana@uou.ac.in

[1] Department of Physics, School of Sciences, Uttarakhand Open University, Haldwani, Uttarakhand 263139, India

behaves as a resonating moiety. This can be considered the main reason for the high chemical reactivity of nitrotoluene. The use of NT and its derivatives are active research trends among researchers. The application of NT as a catalytic reducer was examined (Song et al. 2022). It has potential applications in paints, dyes, rubber, and the leather industry as well. The high electron availability in the benzene ring of NT also leads to its development as a charge transport material (Sangeetha et al. 2018; Pandith and Islam 2014). Thus, the high utilization of NT in industrial applications reflect its potent uses in material science research.

Meanwhile, the requirement for highly efficient nonlinear optical (NLO) materials has given an enormous height to the research field of nonlinear optics. The introduction of new organic NLO materials has revolutionized photonics and optoelectronics. Nonlinear optics is the science that accounts for the collaboration of electromagnetic (EM) light upon the sample (Yadav et al. 1246). The variation of different properties in the sample after introducing it with the EM light leads to their applicability in optical switching, optical power limiting, picture control, telecommunications frequency mixing and generating, photovoltaics and fluorescence, picture preparation, high sensing materials, etc. (Rana et al. 2016; Lakhera et al. 2022a). Modifications in the technology have laid the fact of the high efficiency of the organic NLO materials over the inorganic ones. This has elevated the interest of researchers in developing organic NLO materials. Pyrenes (Felscia et al. 2019), pyrrolidine (Revathi and Rajendran 2018), pyrazine (Jibin et al. 2018), succinimide (Eşme and Sagdinc 2019), anthracenes (Yanxin et al. 2021), quinones (Ejuh et al. 2018), curcumins (Badran et al. 2018), creatininium (Sindhusha et al. 2021), azines (Jessen et al. 2021), pyrrole (Rana et al. 2017), etc., are a few categories of the organic compounds that had been widely worked upon in the past few years. Apart from this, NLO activities of plant-derived compounds like curcumin (Badran et al. 2018), clitorin (Lakhera et al. 2022b), carotenoid (Jeyaram 2022), coriandrum (Sathyavathi et al. 2010), cyclea peltata (Nayak et al. 2021), were also established using the density functional theory (DFT) approach. Moreover, the substitution of halogen had been seen to enormously enhance chemical reactivity. This is probably due to the high chemical reactivity of the halogen atoms. Very high electronegativity of the halogens is also reported which can also be considered as the reason for risen reactivity of the compounds. The availability of the seven valence electrons in the outermost shell of the halogen atoms makes it highly desirable to rapidly complete the octet and attain the stable configuration (Liu et al. 2022). Thus, the halogen-substituted compounds have gained the attention of researchers to a great extent. Literature had reported many studies that accounted for the enhanced NLO activity of molecules right after the substitution of halogens. The research work had been reported for the investigation of NLO activity of the p-iodoaniline and p-bromoaniline (John et al. 1222), Schiff's base material: 4-chloro-4′bromobenzylidene aniline (Sakunthaladevi and Jothi 1233), N-methyl-4-piperiodones curcumin (Sukma et al. 1233), chalcones (Zaini et al. 2019), after the substitution of the halogens. An immense rise in the NLO activity of the molecules was seen in the mentioned studies which motivated us to proceed with the present study.

In the current study, one such aromatic compound has been selected and NLO activity was investigated after substituting the para-position hydrogen with halogen. The study done by D. A. Boateng and team justified the 2NT as a highly reactive molecule and laid the basis of the present study. They used the DFT calculations to explain the radical cation formation from the singlet and triplet 2NT (Boateng et al. 2019). The high reactivity of 4-chloro-2-nitrotoluene was established by V. Krishnakumar and the team using DFT (Krishnakumar et al. 2012). Apart from this, 2NT had been employed for photoluminescence, photothermal activity, dioxygenase enzyme,

dielectric relaxation, and thermodynamically stable agents (Mohan and Malathi 2018; Riega et al. 2013; Parales et al. 2005). The computational investigations on the NLO activities of halogen-substituted 2NT were performed. Theoretical investigations on the structural parameters, spectral properties, and NLO activity were established using DFT.

2 Computational methods

All the computational calculations were performed using Gaussian 09 software packages (https://gaussian.com/) (Frisch 2010). The 3-dimensional geometry of 2NT (PubChem ID: 6944) was downloaded from the database PubChem (https://pubchem.ncbi.nlm.nih.gov/) and the halogens were substituted on the para position of toluene using the builder function over the Gauss View program (https://gaussian.com/gaussview6/) (Dennington et al. 2007). The 2NT has a monoclinic crystal structure ($a \neq b \neq c$, $\alpha = \gamma = 90°$; $\beta > 90°$) with edge length $a = 8.4$, $b = 10.9$, and $c = 15.16$ Å and $\alpha = \gamma = 90°$, $\beta = 105.91°$ (Yakovenko et al. 2009). Halogens are known for their exceptionality of being para-directors despite being highly electronegative atoms. Thus, the para position was better for halogen substitution (Maharramov et al. 2018). The geometry optimization of probe 2NT and 2NT after the substitution of halogens (Cl, F, Br, and I) was performed using DFT with a B3LYP/6-311G++(d,p) set of functions (Becke 1993; Becke and Density-functional thermochemistry. V. 1997). The chemical reactivity and the active participation of the halogen within the 2NT were established using contour plots and chemical reactivity parameters. Different reactivity parameters like bandgap (ΔE), ionization potential (IP), electron affinity (EA), chemical potential (CP), electronegativity (χ), softness (S), and hardness (η) are calculated with the help of Koopman's equations used in previously done studies (Koopmans 1933; Lakhera et al. 2022c, 2022d, 2022e). The molecular orbital map (HOMO–LUMO) and band gap were illustrated using the software Spartan (https://store.wavefun.com/Spartan_Software_s/12.htm). The vibrational activities of the probe and substituted molecules were also examined by computing Raman spectra. The Raman intensity was calculated for high-frequency modes using the expression:

$$I_i = \frac{f\left(\nu_o - \nu_i\right)^4 \mathrm{S}_i}{\nu_i\left[1 - \exp\left(-\frac{hc\nu_i}{\mathrm{kT}}\right)\right]} \tag{1}$$

where I_i is the Raman intensity of the i_{th} vibrational mode, f is a constant with a value of 10^{-12}, and ν_o has a value of 9398.5 cm^{-1}. ν_i and S_i are the vibrational wavenumber and Raman activity of the selected mode respectively. h is Planck constant with value 4.1357×10^{-15} eV s, c is the speed of light having value 3×10^8 m/s, K is Boltzmann constant with value 8.6173×10^{-5} eV K^{-1}, and T is temperature 293.5 K. Time-dependent DFT (TD-DFT) was used for computing the absorption and emission spectra of the probe and substituted molecule with the same set of functions as used for optimization. The values for polarizability parameters like total isotropic polarizability (α_{total}), anisotropy of polarizability ($\Delta\alpha$), and first-order hyperpolarizability (β_{total}) were evaluated for the set of title molecules for the detection of the rise in the NLO activity of the probe 2NT and

halogen-substituted 2NT. These parameters were computed using the equations mentioned in the references (Lakhera et al. 2022f; Ramalingam et al. 2022).

3 Results and discussion

3.1 Structural analysis

The structure optimization was done to the ground state for 2NT and 2NT after the substitution of the halogen atom and the optimized cartesian coordinate has been listed in Table S1, S2, S3, S4, and S5. All the structural parameters like bond lengths and angles were analyzed and listed in Table S6 and S7 respectively. The probe geometry of 2NT was optimized and the computed dipole moment of the molecule was 4.68 Debye. The geometry of 2NT is planar and the methyl group (15H–8C–13H) attached to 4C is a non-planar part. The 16H–9C bond has a bond length of 1.08 Å. The 16H atom attached to the para

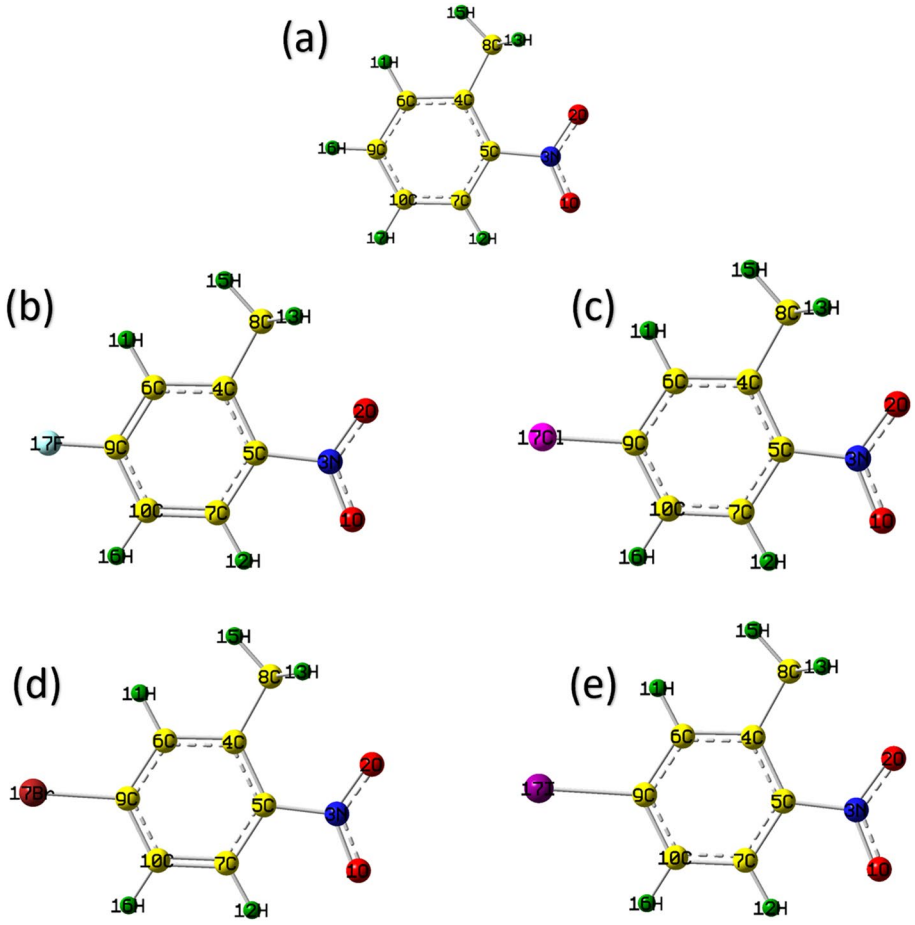

Fig. 1 Optimized geometries of **a** 2NT, **b** 2NT-F, **c** 2NT-Cl, **d** 2NT-Br, and **e** 2NT-I using B3LYP/6-311G++(d,p)

position (9C) of the benzene ring was substituted by the halogen atoms (F, Cl, Br, and I), and the geometries of 2NT-F, 2NT-Cl, 2NT-Br, and 2NT-I are shown on Fig. 1. Halogens are the most electronegative elements of the periodic table. Due to their one valency, they are capable to gain a single electron more easily, increasing the chemical reactivity of the molecule. Thus, the introduction of the halogen into the 2NT molecule results in the increment of the overall chemical reactivity of the complex. Like the probe 2NT, the geometries of 2NT-F, 2NT-Cl, 2NT-Br, and 2NT-I are also planar except for the 15H–8C–13H methyl group that leads to the non-planarity in the complex. The dipole moment of the 2NT seems to rise as the atomic number of the halogen atoms rises. The dipole moments of 2NT-F, 2NT-Cl, 2NT-Br, and 2NT-I were 3.07, 3.5, 3.19, and 3.97 Debye respectively. The bond lengths of 17F–9C, 17Cl–9C, 17Br–9C, and 17I–9C were observed as 1.39, 1.82, 1.94, and 2.13 Å respectively. There seems a rise in the bond length after the introduction of the halogen atom. However, 2NT-I had the largest bond length. The large bond lengths are promising in inducing more chemical reactivity as the large the bond is, easily it will dissociate to give free electrons (Rana and Devlal 2022). So, the increasing bond length from F to I reveals that the 2NT-I can generate a charge cloud more easily. The structural parameters show the enhanced possibility of halogen atoms inducing the intramolecular charge transfer (ICT) within the compounds (Table 1).

3.2 Molecular electrostatic potential surface (MEP)

The MEP surface of the molecules was computed for evidencing the reactiveness. MEP surface identifies the strong nucleophilic sites (negative electrostatic potential) of the molecule that are indicated by the red color and the strong electrophilic (positive electrostatic potential) regions that are indicated by the dark blue color. The yellow and light blue color indicates the partial electrophilic and nucleophilic moieties of the molecule. The MEP surface of the 2NT indicates the nucleophilic behavior of the nitro group and the electrophilic nature of the hydrogen atoms attached to the carbon atoms of the benzene ring. After the substitution of the halogen atoms, the MEP surface indicates the participation of the halogen atoms in charge delocalization (Fig. 2).

3.3 Mulliken charge and contour plots analysis

The charge distribution was also examined for the 2NT-F, 2NT-Cl, 2NT-Br, and 2NT-I and the Mulliken charge distribution of these molecules are listed in Table S8. The Mulliken charge distribution of the molecules shows the negative charge contribution of the oxygen and nitrogen atoms. The hydrogen atoms, however, contribute positively. The 9C atom attached to the para hydrogen 16H has a negative charge of − 0.111e. This charge seems to decrease as the atomic number of the halogens increases. This can be due to the decreasing order of electronegativity of the halogen atoms i.e., F > Cl > Br > I. The 17H atom has a positive charge of 0.167e. The 17F has a negative charge (− 0.323 e) but the rest of the halogen atoms impart positively (17Cl (0.012e), 17Br (0.216 e), 17I (0.165 e)) in the total charge of the molecules. There seems a huge charge variation in the Mulliken charge among the halogenated hydrogen and the nitro group. This variation identifies the intramolecular interaction within the molecules (Lakhera et al. 2021). The chemical reactivity was also verified by contour maps of the molecules (Fig. 3). The contour maps generally symbolize the behavior of the field lines when the material is placed in the electrostatic field (Khan et al. 2022). The gathering of field lines near

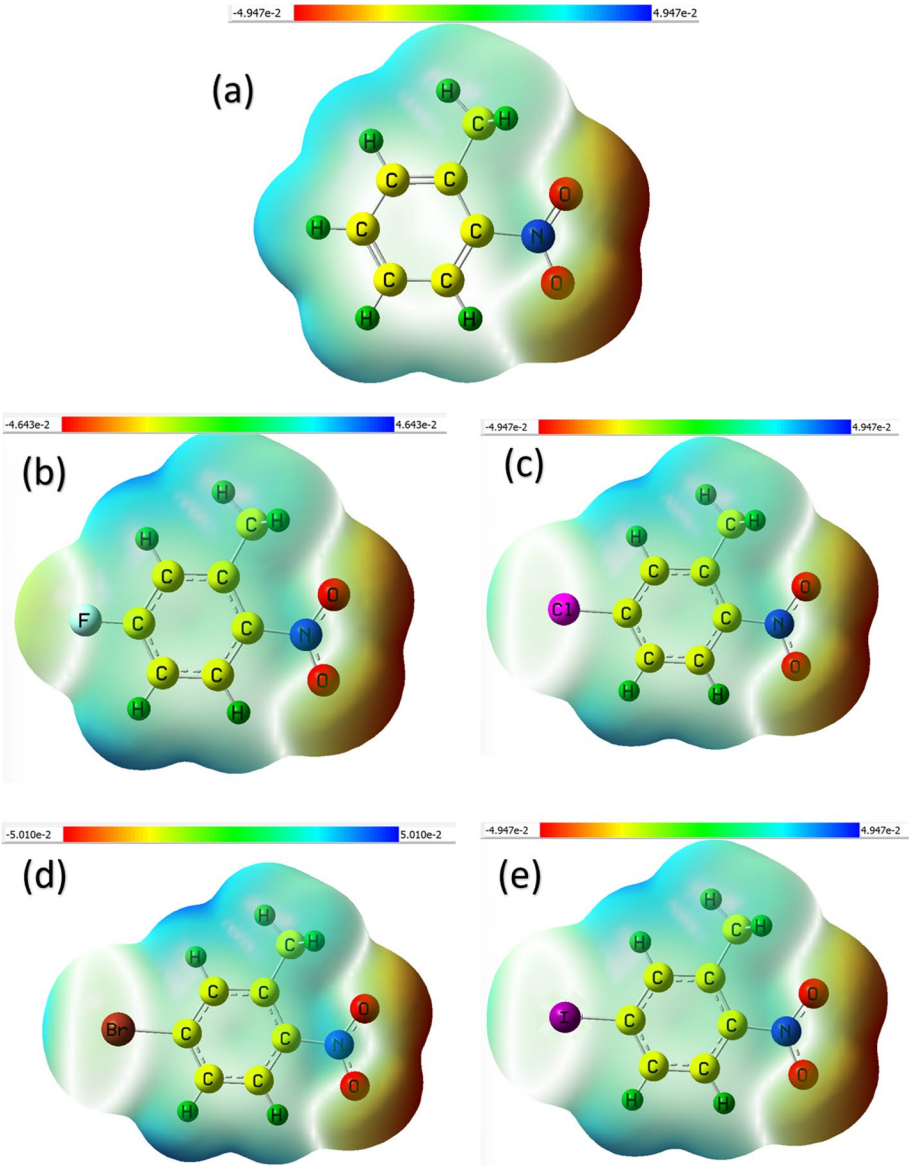

Fig. 2 Molecular electrostatic potential surface of **a** 2NT, **b** 2NT-F, **c** 2NT-Cl, **d** 2NT-Br, and **e** 2NT-I using B3LYP/6-311G++(d,p)

the nitro group in 2NT shows that this area is highly under influence of the electrostatic field. The bonds settled near such areas experience regular stretching and shrinking of the bonds resulting in the weakening of the bonds (Weeraratna et al. 2021). Such bonds have more probability of undergoing dissociation resulting in the evolution of a charge cloud. The red contour lines indicate the electron-donating part. Thus, a free-charge cloud is seen to generate from the nitro group. The substitution of halogens enhanced

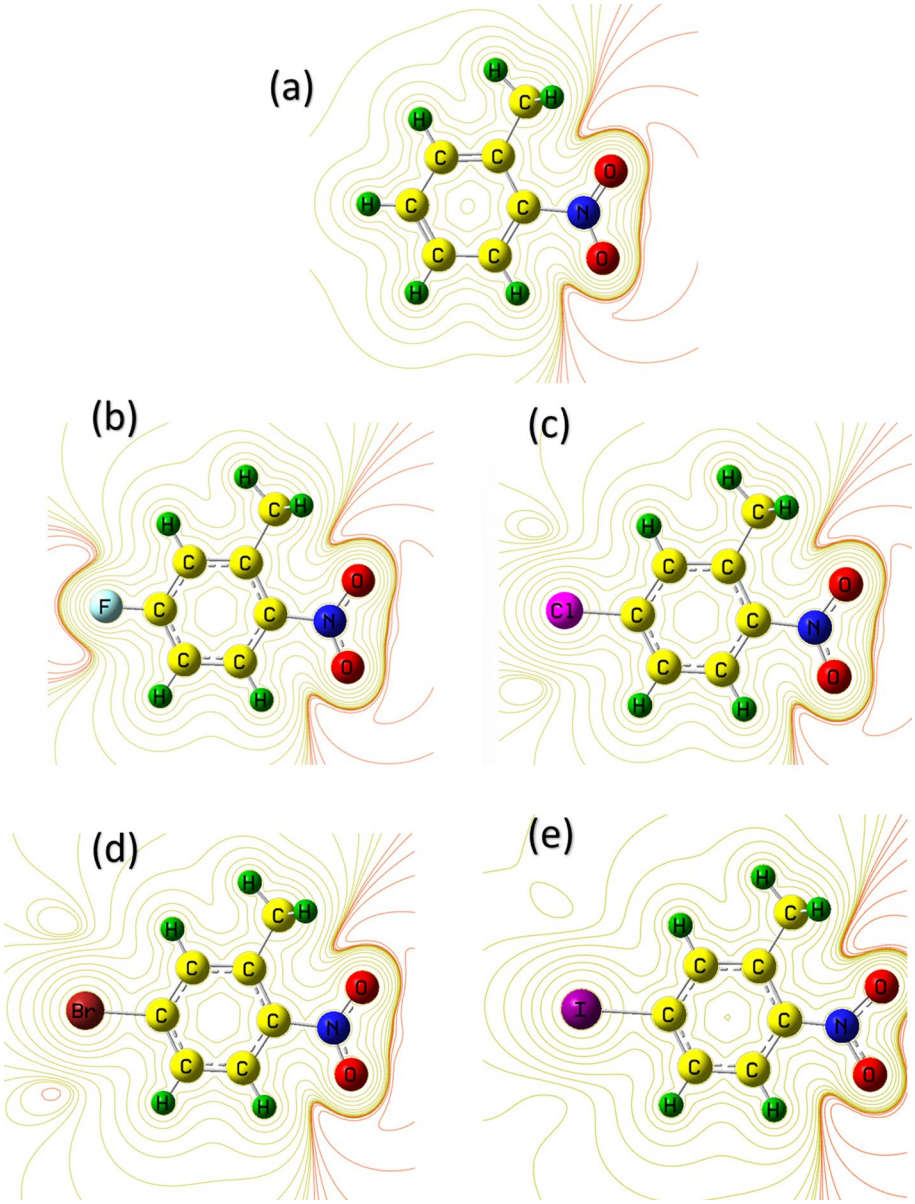

Fig. 3 Contour lines of **a** 2NT, **b** 2NT-F, **c** 2NT-Cl, **d** 2NT-Br, and **e** 2NT-I using B3LYP/6-311G++(d,p). Red color lines indicate the electropositive and yellow color indicates the electronegative part of the molecules

the ability of ICT. The contour plots of the halogen-substituted molecules (Fig. 3b, c, d, and e) exhibits the highly accumulated yellow lines surrounding the halogen atoms showing the electron-withdrawing behavior of the halogen atoms. It reveals the active participation of the halogens in accepting the charge cloud. Thus, the contour plots

Table 1 Variation in the bond lengths of halogen substituted location in (a) 2NT, (b) 2NT-F, (c) 2NT-Cl, (d) 2NT-Br, and (e) 2NT-I using B3LYP/6-311G++(d,p) (bond length is in Å)

Compound	Bond	Bond length
2NT	9C–16H	1.08
2NT-F	17F–16H	1.39
2NT-Cl	17F–16H	1.82
2NT-Br	17F–16H	1.94
2NT-I	17I–16H	2.13

indicated the dislocation of the charge cloud from the nitro group towards the halogen atoms. Therefore, the Mulliken charge distribution and the contour plots convey that the introduction of the halogen atoms enhances the ability of the molecules to induce ICT within the molecules.

3.4 Molecular orbital analysis

Molecular orbital parameters are computed in the study to investigate the chemical reactivity and the values are listed in Table 2. The energies corresponding to HOMO–LUMO were used to compute the global reactivity parameters. The ΔE of the halogen-substituted molecules decreases with the increase in the atomic number of the halogens. The low ΔE value for 2NT-I shows the easy drifting of the electrons from lower energy orbitals to higher energy orbitals. *IP* is the minimum energy that is required to eject the outermost valence electrons. Among halogen-substituted atoms, 2NT-I has the minimum value of 7.39 eV for *IP* which reveals the tendency of 2NT-I to ionize valence electrons more easily than the other halogen compounds. The high value of *EA* reveals the capability of the molecule to attract the free electron pairs. The values of *EA* increases as 2NT-F < 2NT-Br < 2NT-I < 2NT-Cl. The CP value is also higher for 2NT-I (− 5.34 eV), showing its active participation in the chemical reactions than the other halogen-substituted molecules. The high values of χ reveals the high chemical reactivity of the molecules. The halogens are known to be highly reactive and thus have high values of χ. Br < I < F < Cl is the order of χ. The chemical hardness (η) defines the rigidness of the molecules. 2NT-F has the highest chemical hardness among the other halogen-substituted molecules. In contrast, the low

Table 2 FMO parameters for the (a) 2NT, (b) 2NT-F, (c) 2NT-Cl, (d) 2NT-Br, and (e) 2NT-I molecule (all values in eV and value of S is in eV^{-1})

S No	Molecular property	2NT	2NT-F	2NT-Cl	2NT-Br	2NT-I
1	E_{HOMO}	− 7.61	− 7.87	− 7.80	− 7.60	− 7.39
2	E_{LUMO}	− 2.78	− 2.89	− 3.31	− 2.99	− 3.30
3	Energy gap (ΔE)	4.83	4.98	4.49	4.61	4.09
4	Ionization potential (*IP*)	7.61	7.87	7.80	7.60	7.39
5	Electron affinity (*EA*)	2.78	2.89	3.31	2.99	3.30
6	Chemical potential (*CP*)	− 5.19	− 5.38	− 5.55	− 5.29	− 5.34
7	Electronegativity (χ)	5.19	5.38	5.55	5.29	5.34
8	Chemical hardness (η)	2.41	2.49	2.24	2.3	2.04
9	Softness (*S*)	0.41	0.4	0.44	0.43	0.49

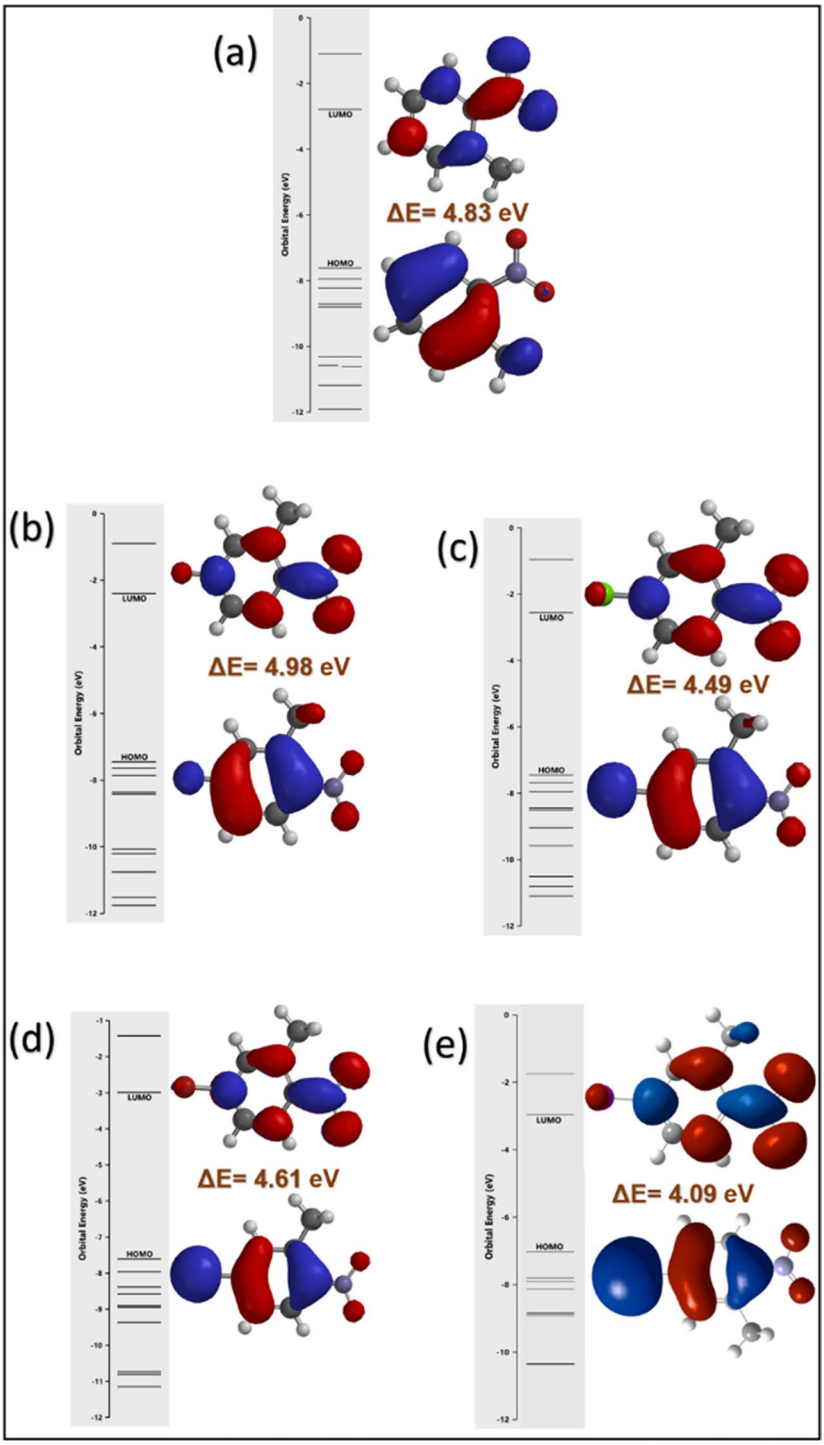

Fig. 4 Molecular orbitals for the **a** 2NT, **b** 2NT-F, **c** 2NT-Cl, **d** 2NT-Br, and **e** 2NT-I. The lower structure shows HOMO and upper structure shows LUMO of the respective molecules and the band gap is represented by ΔE

value of *S* reveals the chemical stability of the molecule, which is lowest for 2NT-F and 2NT-I. The uniformly distributed HOMO–LUMO map of the molecules is shown in Fig. 4. The blue color indicates the donating (i.e., positive) moieties and the red color indicates the electron-withdrawing (i.e., negative) moieties of the molecules (Morosanu et al. 2017). The unavailability of the HOMO–LUMO surface over the 16H atom at the para position of the 2NT indicates that it does not participate in the charge transfer, but as the 16H was substituted by the halogen atoms, the shifting of HOMO–LUMO surfaces over the halogen atoms was observed. This indicates the active participation of the halogen atoms in ICT. The red color surface over the halogens shown in Figs. 4b, c, d, and e, reveals that the halogen atoms readily behave as the strong electron-withdrawing moieties in the molecules. This is obviously due to the high electronegative nature of the halogens. There seems a shifting of charge cloud in halogen-substituted 2NT that shows the enhanced chemical reactivity of these molecules. Thus, the frontier molecular orbital (FMO) and HOMO–LUMO analysis highlight the rise in the active chemical reactivity of the 2NT molecule after the substitution of the halogen atoms. Although, the 2NT-I has comparatively higher chemical reactivity than the other halogen-substituted 2NT molecules. This is also in better agreement with the high possibility of ICT in 2NT-I stated by structural and charge analysis.

3.5 Absorption and emission analysis

The simulated absorption spectra for halogen-substituted 2NT were computed using TD-DFT and illustrated in Fig. 5 and the transition details are mentioned in Table S9. It is clearly observable that the absorbance intensity of the 2NT molecule increases after the substitution of the halogens. Along this, a rise in absorption peak was also observed for halogen-substituted 2NT. The high electronegativity of the halogens leads to the rise in the wavelengths of electronic transitions within the 2NT-F, 2NT-Cl, 2NT-Br, and 2NT-I molecules. The $S_0 = > S_1$ transition for 2NT was observed at wavelength 386 nm. This value changes to 385, 387, 388, and 390 nm for 2NT-F, 2NT-Cl, 2NT-Br, and 2NT-I molecules respectively. The excitation from HOMO-2 to LUMO in 2NT is responsible

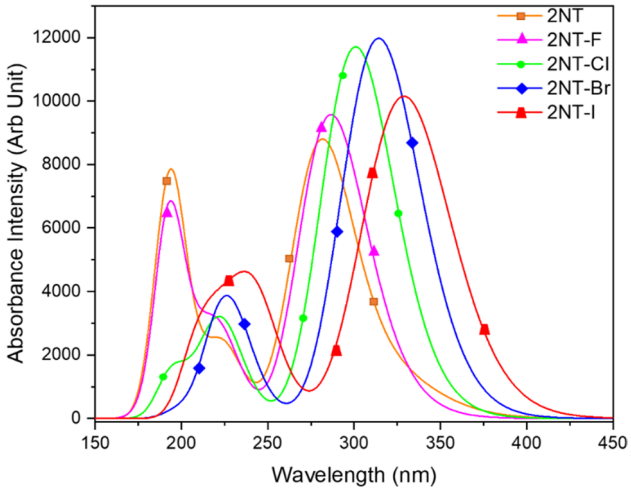

Fig. 5 Absorption spectra of the **a** 2NT, **b** 2NT-F, **c** 2NT-Cl, **d** 2NT-Br **e** 2NT-I computed using B3LYP/6-311G++(d,p) basis set

for the $S_0 => S_1$ transition. After the substitution of the F atom, the $S_0 => S_1$ transition occurred due to the excitation from HOMO-4 to LUMO. In the case of 2NT-Cl and 2NT-Br, the $S_0 => S_1$ transition was observed due to the excitation between HOMO-2 to LUMO. The $S_0 => S_1$ transition in 2NT-I was observed due to the excitation between HOMO-3 to LUMO. Among 2NT, 2NT-F, 2NT-Cl, 2NT-Br, and 2NT-I, 2NT-I had the maximum wavelength of the absorption spectra. The wavelength of $S_0 => S_1$ transition in 2NT-I was reported at 390 nm showing the existence of typical $\pi \rightarrow \pi^*$ transitions (Rana et al. 2021). Thus, the absorbance spectra analysis reported that 2NT-I has an absorption band with the highest wavelength which leads to high chemical reactivity and thus, high polarizability of the 2NT-I.

The details of the transitions of emission spectra of all the molecules had been mentioned in Table S10. The peaks of the emission spectra were at higher wavelengths than the absorption spectra. $S_0 <= S_1$ transition of 2NT and 2NT after the substitution of halogens occurred for the HOMO to LUMO excitation. The $S_0 <= S_1$ emissive transition for 2NT was observed at 718 nm. This value increases after the substitution of halogen atoms. The wavelength of $S_0 <= S_1$ transition for 2NT-F, 2NT-Cl, 2NT-Br, and 2NT-I were recorded as 712, 722, 723, and 748 nm respectively. 2NT-I has the highest wavelength recorded for emission as compared to the 2NT, 2NT-F, 2NT-Cl, and 2NT-Br. The radiative lifetime (τ) for observing the emissive nature of the transitions can be obtained by the below-given formula (Rana and Chowdhury 2015):

$$\tau = \frac{c^3}{2fE^2} \tag{2}$$

where c is the speed of light, f and E are the oscillator strength and the excitation energy. The value of τ reveals whether the molecules emit radiation during the transitions or whether the transitions are non-radiative. However, the 0.000 value of oscillator strength was observed for the $S_0 <= S_1$ transition for all the title molecules, i.e., these transitions are dark transitions. To the contrary, the denominator of (2) equates to zero which gives an infinite value for τ. Thus, the emission analysis indicates the zero-quantum yield for 2NT in the probe state and after the substitution of halogen atoms.

3.6 Vibrational analysis

Vibrational modes were analyzed for major modes of the title molecules. Figure 6 illustrates a fair comparison between the simulated vibrational spectra. The unavailability of any imaginary frequencies in the vibrational modes confirms the optimized geometry corresponds to a minimum (Lakhera et al. 2023). The detailed modes were mentioned in Table S11. The linear symmetric stretching (ν) of para C–H bond was observed around 1230.33 cm^{-1}. After the substitution of the halogen, there seems a rise in the Raman intensity of the bond. The ν mode of C–F, C–Cl, C–Br, and C–I was observed at 1256.76, 1271.48, 1271.16, and 1284.74 cm^{-1} respectively. The symmetric bending of C–C bonds of the benzene ring was observed between 1300 and 1600 cm^{-1} for all the molecules. The intensity, however, seems to rise with the rise in the atomic number of halogens (say F < Cl < Br < I). The asymmetric stretching (α) of C–H bonds were observed above 3000 cm^{-1} and gradually increase from F to I. The other important modes are defined in Fig. 6. As the high Raman intensity leads to the high polarizability of the molecules (Lakhera et al. 2022g; Ojo et al. 2020; Moroz and Edwards 2021).

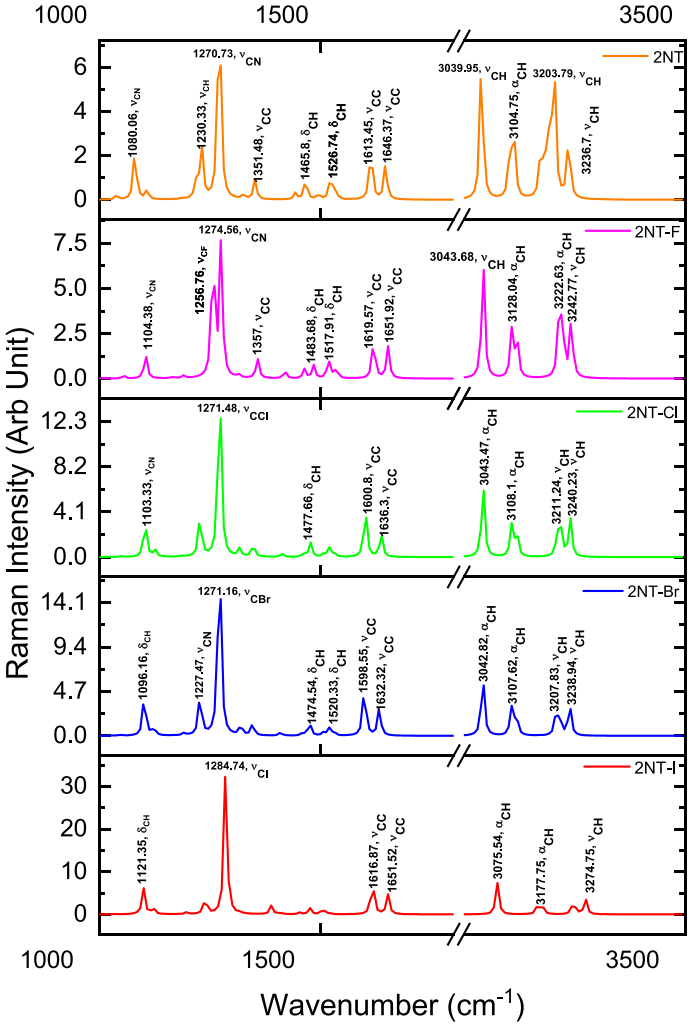

Fig. 6 Vibrational spectra for the **a** 2NT, **b** 2NT-F, **c** 2NT-Cl, **d** 2NT-Br **e** 2NT-I molecule computed using B3LYP/6-311G++(d,p) basis set (Symmetric stretching-ν, asymmetric stretching-α, symmetric bending in the plane (scissoring)-δ

The gradual rise in the Raman intensity of the vibrational modes related to the nitro group and halogen atom indicates the high polarizability of the halogen-substituted NT molecule.

3.7 NLO analysis

The computed polarizability parameters were to develop the molecule's NLO activities. These polarizability parameters are actually the coefficients of the Taylor series expansion of the energy of a material placed in the electromagnetic field and their higher magnitudes are responsible for the NLO activity of the materials (Bhatt et al. 2020). The tensor

Table 3 Computed values of the α_{total}, $\Delta\alpha$, and β_{total} for the (a) 2NT, (b) 2NT-F, (c) 2NT-Cl, (d) 2NT-Br, and (e) 2NT-I (All values are in esu)

Molecule	α_{total}	$\Delta\alpha$	β_{total}
2NT	12.95×10^{-24}	31.64×10^{-24}	2.81×10^{-30}
2NT-F	13.06×10^{-24}	32.62×10^{-24}	5.42×10^{-30}
2NT-Cl	14.94×10^{-24}	41.93×10^{-24}	9.54×10^{-30}
2NT-Br	15.87×10^{-24}	45.73×10^{-24}	12.37×10^{-30}
2NT-I	16.64×10^{-24}	51.55×10^{-24}	18.72×10^{-30}

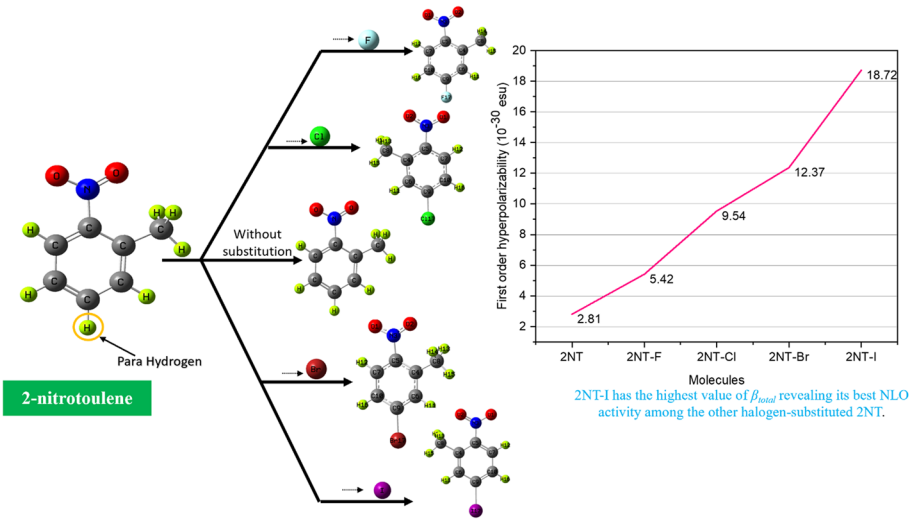

Fig. 7 Comparative plot illustrating the rise in the hyperpolarizability of 2NT after substituting halogen atoms

components of the polarizability and hyperpolarizability are listed in Table S12 and S13 respectively. The values of α_{total}, $\Delta\alpha$, and β_{total} for 2NT were computed as 12.95×10^{-24}, 31.64×10^{-24}, and 2.81×10^{-30} esu respectively. There seems a rise in the values of the polarizability parameters after the substitution of the halogen atom. Moreover, the respective values rise as the atomic number of the halogen atoms rises, i.e., the values of polarizability parameters increase as the atomic number rises. The values of polarizability parameters are listed in Table 3. The values of α_{total} for 2NT-F, 2NT-Cl, 2NT-Br, and 2NT-I are in increasing order of 13.06×10^{-24}, 14.94×10^{-24}, 15.87×10^{-24} and 16.64×10^{-24} esu respectively (Fig. 6). Similarly, the values of $\Delta\alpha$ are also in increasing order of 2NT-F (31.64×10^{-24} esu) < 2NT-Cl (32.62×10^{-24}esu) < 2NT-Br (41.93×10^{-24} esu) < 2NT-I (45.73×10^{-24}esu). β_{total} is the parameter that mainly constitutes the NLO activity of the molecule. 2NT-I (18.72×10^{-30} esu) has the highest value of β_{total} compared to 2NT-F (5.42×10^{-30} esu), 2NT-Cl (9.54×10^{-30} esu), and 2NT-Br (12.37×10^{-30} esu). The introduction of halogens into 2NT shows an immense rise in the β_{total} that reveals their high ability to act as NLO material (Fig. 7). This might be due to the high chemical reactivity of the halogens. Although, the Iodine-substituted 2NT molecule has the best potentiality of an NLO active molecule other than the F, Cl, and Br compounds. For better validation of the results, the β_{total} was compared with the most generally used reference material Urea

(0.781×10^{-30} esu) (Singla et al. 2015). The β_{total} of 2NT-I seems to be 24 times higher than Urea and two and a half times higher than KDP which shows the high NLO activity of the 2NT-I molecule. The computed results are compared with halogen-substituted *N*-methyl-4-piperidone curcumin derivatives mentioned in the reference study (Sukma et al. 1233). The values of the β_{total} for 10 different halogen-substituted compounds ranged from 6.62×10^{-30} esu to 13.005×10^{-30} esu (Cassidy et al. 1979). These values are comparatively less than the β_{total} of 2NT-I. Thus, the present study conveys the NLO activity of the halogen-substituted molecules.

4 Conclusion

The substitution of halogens in the 2NT molecule has enormously scaled the quantum mechanical properties of the 2NT. This was due to the high electronegativity of the halogens. The rise in the structural parameters and FMO parameters was observed due to the electronegativity of the halogens. Large variation in the charges of the atoms and the accumulation of the field lines near the halogen atoms justifies the active participation of the halogens in inducing the intramolecular interactions and shifting of charge cloud from the nitro group towards the halogen atom. The absorbance intensity also undergoes a rise after the substitution of the halogens and increases with the increasing atomic number of the halogens i.e., F < Cl < Br < I. Thus, the highest absorbance intensity was observed for the 2NT-I molecule. The computed values of the radiative lifetime for crucial transitions reveal the radiative nature of transitions. A similar kind of rise was observed in the Raman intensity after the substitution of the halogens. The 2NT-I has the vibrational modes with the highest Raman intensity. The values of the β_{total} of the 2NT-F, 2NT-Cl, 2NT-Br, and 2NT-I are computed to be three times, seven times, twelve times, and twenty-four times higher than Urea. Thus, from the present study, it can be concluded that the halogen-substituted 2NT molecules possess promising NLO activity. In comparison, the 2NT-I has the highest value of β_{total} revealing its best NLO activity among the other halogen-substituted 2NT. We believe that the halogen-substituted 2NT has proven to be an excellent candidate for promoting the upgrading and updating of NLO devices with greatly improved performance and novel functionalities. Moreover, the experimental demonstration of the present study will surely be rewarding.

Supplementary Information The online version contains supplementary material available at https://doi.org/10.1007/s11082-023-04569-3.

Author contributions SL: Data curation, Writing-Original draft preparation, Visualization, Investigation, Software, Validation. MR: Conceptualization, Methodology, Writing-Reviewing and Editing, Supervision. KD: Conceptualization, Writing- Reviewing and Editing.

Funding The authors declare that this research received no specific grant from any funding agency.

Availability of data and materials All data generated or analysed during this study, which support the plots within this paper and the other findings of this study, are included in this article and it is Supplementary Information. Source data are provided with this paper.

Declarations

Conflict of interest The authors declare that they have no known competing financial interests or personal relationships that could have appeared to influence the work reported in this paper.

Ethical approval This material is the authors' own original work, which has not been previously published elsewhere. All authors have been personally and actively involved in substantial work leading to the paper and will take public responsibility for its content. The paper properly credits the meaningful contributions of all the co-authors.

References

Badran, H.A., Al-Maliki, A., Alfahed, R.K.F., et al.: Synthesis, surface profile, nonlinear reflective index and photophysical properties of curcumin compound. J. Mater. Sci. Mater. Electron. **29**, 10890–10903 (2018). https://doi.org/10.1007/s10854-018-9167-0

Bhatt, T., Pant, T., Dhondiyal, C.C., Rana, M., Chowdhury, P., Joshi, G.C., Arya, G.C., Tiwari, H.: Computational study of the intermolecular interactions and their effect on the UV–visible spectra of the ternary liquid mixture of benzene, ethanol and propylene glycol. J Mol. Model. **26**, 268 (2020). https://doi.org/10.1007/s00894-020-04533-y

Becke, A.D.: Density-functional thermochemistry. III. The role of exact exchange. J. Chem. Phys. **98**, 5648 (1993). https://doi.org/10.1063/1.464913

Becke, A.D.: Density-functional thermochemistry. V. Systematic optimization of exchange-correlation functionals. J. Chem. Phys. **107**, 8554–8560 (1997). https://doi.org/10.1063/1.475007

Boateng, D.A., Kayla, M., Word, D., Gutsev, L.G., Jena, P., Tibbetts, K.M.: Conserved vibrational coherence in the ultrafast rearrangement of 2-nitrotoluene radical cation. J. Phys. Chem. A **123**(6), 1140–1152 (2019). https://doi.org/10.1021/acs.jpca.8b11723

Cassidy, C., Halbout, J.M., Donaldson, W., Tang, C.L.: Nonlinear optical properties of urea. Opt. Commun. **29**(2), 243–246 (1979). https://doi.org/10.1016/0030-4018(79)90027-0

Dennington, R., Keith, T., Millam, J.: GaussView, Version 4.1.2, Semichem, Inc., Shawnee Mission, KS (2007).

Ejuh, G.W., Nya, F.T., Djongyang, N., et al.: Study of some properties of quinone derivatives from quantum chemical calculations. Opt. Quantum Electron. **50**, 336 (2018). https://doi.org/10.1007/s11082-018-1603-0

Eşme, A., Sagdinc, S.G.: Conformational, spectroscopic (FT-IR, FT-Raman, and UV–Vis), and molecular docking studies of N-(2-hydroxyethyl) succinimide. J. Mol. Struct. **1195**, 451–461 (2019). https://doi.org/10.1016/j.molstruc.2019.06.019

Felscia, U.R., Rajkumar, B.J.M.: Computational study of quinacridone on silver and gold clusters: applications to organic light emitting diodes and nonlinear optical devices. Mater. Lett. (2018). https://doi.org/10.1016/j.matlet.2018.03.149

Felscia, U.R., Rajkumar, B.J.M., Sankar, P., Philip, R., Mary, M.B.: Theoretical and experimental investigations of nitropyrene on silver for nonlinear optical and metal ion sensing applications. Mater. Chem. Phys. (2019). https://doi.org/10.1016/j.matchemphys.2019.122466

Frisch, M.J.: Gaussian 09, Revision B.01, Gaussian Inc., Wallingford CT (2010).

Jessen, N.I., Bertuzzi, G., Bura, M., Skipper, M.L., Jørgensen, K.L.: Enantioselective construction of the Cycl[3.2.2]azine core via organocatalytic [12 + 2] cycloadditions. J. Am. Chem. Soc (2021). https://doi.org/10.1021/jacs.1c00499

Jeyaram, S.: Spectral, third-order nonlinear optical and optical switching behavior of β-carotenoid extracted from phyllanthus niruri. Indian J Phys. **96**, 1655–1661 (2022). https://doi.org/10.1007/s12648-021-02122-0

Jibin, S., Yantao, S., Chaoxian, Y., Dongxu, L., Zheng, X., Shuyun, Z., Chengshan, Y., Li, Z.H., Xiangfeng, S.: Remarkable nonlinear optical response of pyrazine-fused trichalcogenasumanenes and their application for optical power limiting. J. Mol. Struct. **6**(48), 13114–13119 (2018). https://doi.org/10.1039/c8tc04778b

John, N.L., Abraham, S., Sajan, D., Sarojini, B.K., Narayana, B.: Quantum chemical studies of molecular structure, vibrational spectra and nonlinear optical properties of p-iodoaniline and p-bromoaniline. J. Mol. Struct. **1222**, 128939 (2020). https://doi.org/10.1016/j.molstruc.2020.128939

Khan, M.U., Khalid, M., Khera, R.A., Akhtar, M.N., Abbas, A., Rehman, M.F., Braga, A.A.C., Alam, M.M., Imran, M., Wang, Y., Lu, C.: Influence of acceptor tethering on the performance of nonlinear optical properties for pyrene-based materials with A-π-D-π-D architecture. Arab. J. Chem. **15**(3), 103673 (2022). https://doi.org/10.1016/j.arabjc.2021.103673

Koopmans, T.: Ordering of wave functions and eigenenergies to the individual electrons of an atom. Physica **1**, 104–113 (1933). https://doi.org/10.1016/S0031-8914(34)90011-2

Krishnakumar, V., Murugeswari, K., Prabavathi, N., Mathammal, R.: Molecular structure, vibrational spectra, HOMO, LUMO and NMR studies of 2-chloro-4-nitrotoluene and 4-chloro-2-nitrotoluene. Spectrochim. Acta A Mol. **91**, 1–10 (2012). https://doi.org/10.1016/j.saa.2012.01.038

Lakhera, S., Devlal, K., Ghosh, A., Rana, M.: In silico investigation of phytoconstituents of medicinal herb 'Piper Longum' against SARS-CoV-2 by molecular docking and molecular dynamics analysis. Results Chem. **3**, 100199 (2021). https://doi.org/10.1016/j.rechem.2021.100199

Lakhera, S., Rana, M., Devlal, K.: Theoretical study on spectral and optical properties of essential amino acids: a comparative study. Opt. Quantum Electron. **54**, 714 (2022a). https://doi.org/10.1007/s11082-022-04118-4

Lakhera, S., Devlal, K., Rana, M., Celik, I.: Study of nonlinear optical responses of phytochemicals of *Clitoria ternatea* by quantum mechanical approach and investigation of their anti-Alzheimer activity with in silico approach. Struct. Chem. (2022b). https://doi.org/10.1007/s11224-022-01981-5

Lakhera, S., Devlal, K., Rana, M., Dhuliya, V.: Quantum mechanical study of three aromatic bioactive fatty alcohol compounds with nonlinear optical and potential light harvesting properties. Opt. Mater. **129**, 112476 (2022c). https://doi.org/10.1016/j.optmat.2022.112476

Lakhera, S., Rana, M., Devlal, K.: Modelling the reactivity of entrectinib and evaluation of its potential anticancer activity using molecular docking approach. DAE Solid State Phys. Symp **55**, 583–584 (2022d)

Lakhera, S., Devlal, K., Ghosh, A., Rana, M.: Modelling the DFT structural and reactivity study of feverfew and evaluation of its potential antiviral activity against COVID-19 using molecular docking and MD simulations. Chem. Pap. **76**, 2759–2776 (2022e). https://doi.org/10.1007/s11696-022-02067-6

Lakhera, S., Rana, M., Devlal, K., Celik, I., Yadav, R.: A comprehensive exploration of pharmacological properties, bioactivities and inhibitory potentiality of luteolin from *Tridax procumbens* as anticancer drug by in-silico approach. Struct. Chem. (2022f). https://doi.org/10.1007/s11224-022-01882-7

Lakhera, S., Rana, M., Devlal, K.: Investigation of nonlinear optical response of organic compound pyrrolidine-2,5-dione. DAE Solid State Phys. Symp. **55**, 585–586 (2022g)

Lakhera, S., Rana, M., Devlal, K.: Influence of adsorption of gold and silver nanoclusters on structural, electronic, and nonlinear optical properties of pentacene-5,12-dione: a DFT study. Opt. Quant. Electr. **55**,178 (2023). https://doi.org/10.1007/s11082-022-04422-z

Lin, M.F., Lee, Y.E., Ni, C.K., Xu, S., Lin, M.C.: Photodissociation dynamics of nitrobenzene and o-nitrotoluene. Chem. Phys. **126**(6), 064310 (2007). https://doi.org/10.1063/1.2435351

Liu, Y., Wang, R., Wang, Z., et al.: Formation of twelve-fold iodine coordination at high pressure. Nat. Commun. **13**, 412 (2022). https://doi.org/10.1038/s41467-022-28083-4

Maharramov, A.M., Shikhaliyev, N.Q., Suleymanova, G.T., Gurbanov, A.V., Babayeva, G.V., Mammadova, G.Z., Zubkov, F.I., Nenajdenko, V.G., Mahmudov, K.T., Pombeiro, A.J.L.: Pnicogen, halogen and hydrogen bonds in (E)-1-(2,2-dichloro-1-(2-nitrophenyl)vinyl)-2-(para-substituted phenyl)-diazenes. Dyes Pigments **159**, 135–141 (2018). https://doi.org/10.1016/j.dyepig.2018.06.022

Majee, P., Singha, D.K., Mondal, S.K., Mahata, P.: Effect of charge transfer and structural rigidity on divergent luminescence response of a metal organic framework towards different metal ions: luminescence lifetime decay experiments and DFT calculations. PPS (2019). https://doi.org/10.1039/C9PP00024K

Mohan, A., Malathi, M.: Dielectric relaxation and thermodynamic studies of binary mixtures of 2-nitrotoluene with primary and secondary alcohols at different temperatures. J. Solut. Chem. **47**, 667–683 (2018). https://doi.org/10.1007/s10953-018-0744-x

Morosanu, A., Cezarina, B., Andreea, C., Babusca, D., Dimitriu, D.G., Dorohoi, O.D.: Quantum mechanical and solvatochromic characterization of quercetin. Anal. Lett. **50**(17), 2725–2739 (2017). https://doi.org/10.1080/00032719.2017.1291657

Moroz, T.N., Edwards, H.G.M.: The use of Raman and infrared spectroscopy in determining the space symmetry group among the groups with the same rules of systematic absence in the diffraction patterns: some basic principles and applications. J. Raman Spectrosc. **52**, 2058–2067 (2021). https://doi.org/10.1002/jrs.6220

Nayak, S., Manjunatha, K.B., Goveas, L.C., et al.: Investigation of nonlinear optical properties of AgNPs synthesized using *Cyclea peltata* leaf extract post OVAT optimization. BioNanoScience **11**, 884–892 (2021). https://doi.org/10.1007/s12668-021-00875-w

Ojo, N.D., Krause, R.W., Obi-Egbedi, N.O.: Electronic and nonlinear optical properties of 3-(((2-substituted-4-nitrophenyl)imino)methyl)phenol. Comput. Theor. Chem. **1192**, 1–8 (2020). https://doi.org/10.1103/PhysRevX.11.021067

Pandith, A.H., Islam, N.: Electron transport and nonlinear optical properties of substituted aryldimesityl boranes: a DFT study. PLoS ONE **9**(12), e114125 (2014). https://doi.org/10.1371/journal.pone.0114125

Parales, R.E., Huang, R., Yu, C.L., Parales, J.V., Lee, F.K.N., Lessner, D.J., Ivkovic-Jensen, M.M., Liu, W., Friemann, R., Ramaswamy, S., Gibson, D.T.: Purification, Characterization, and crystallization of the components of the nitrobenzene and 2-nitrotoluene dioxygenase enzyme systems. Appl. Environ. Microbiol. **71**(7), 3806–3814 (2005). https://doi.org/10.1128/AEM.71.7.3806-3814.2005

Ramalingam, A., Kuppusamy, M., Sambandam, S., Medimagh, M., Oyeneyin, O.E., Shanmugasundaram, A., Issaoui, N., Ojo, N.D.: Synthesis, spectroscopic, topological, hirshfeld surface analysis, and anti-covid-19 molecular docking investigation of isopropyl 1-benzoyl-4-(benzoyloxy)-2,6-diphenyl-1,2,5,6-tetrahydropyridine-3-carboxylate. Heliyon **8**(10), e10831 (2022). https://doi.org/10.1016/j.heliyon.2022.e10831

Rana, M., Chowdhury, P.: L-glutathione capped CdSeS/ZnS quantum dots as an environmentally hazardous chemical sensor. J. Appl. Eng. **2**(16), 1319–1321 (2015)

Rana, M., Devlal, K.: Thioglycolic acid capped CdTe quantum dots as sensors for the detection of hazardous heavy metal ion Cu^{2+} in water. Mapan **37**, 41–46 (2022). https://doi.org/10.1007/s12647-021-00479-5

Rana, M., Singla, N., Chatterjee, A., Shukla, A., Chowdhury, P.: Investigation of nonlinear optical (NLO) properties by charge transfer contributions of amine-functionalized tetraphenylethylene. Opt. Mater. **62**, 80–89 (2016). https://doi.org/10.1016/j.optmat.2016.09.043

Rana, M., Singla, N., Pathak, A., Dhanya, R., Narayana, C., Chowdhury, P.: Vibrational-electronic properties of intra/inter molecular hydrogen bonded heterocyclic dimer: an experimental and theoretical study of pyrrole-2-carboxaldehyde. Vib. Spectrosc. **89**, 16–25 (2017). https://doi.org/10.1016/j.vibspec.2016.12.003

Rana, M., Banerjee, C., Chowdhury, P.: Studies on optical signal due to oxygen effect on hydrogenated amorphous/crystalline silicon thin films. Appl. Phys. a. **127**, 192 (2021). https://doi.org/10.1007/s00339-021-04322-1

Revathi, V., Rajendran, V.: Investigation about nonlinear optics and antibacterial activity of pyrrolidine-2-carboxylic acid cadmium chloride hydrate single crystal. Optik **154**, 234–241 (2018). https://doi.org/10.1016/j.ijleo.2017.10.060

Riega, H.D., Gunawidjaja, R., Eilers, H.: Photoluminescence spectroscopy of 2-nitrotoluene and its photo and photothermal decomposition derivatives. J. Photochem. Photobiol. **268**, 50–57 (2013). https://doi.org/10.1016/j.jphotochem.2013.06.020

Sakunthaladevi, R., Jothi, L.: Chemical growth dynamics of 4-methyl-4′-hydroxy benzylidene aniline NLO single crystal structure and spectroscopic applications. J. Mol. Struct. **1233**, 130054 (2021). https://doi.org/10.1016/j.molstruc.2021.130054

Sangeetha, K., Prasad, L.G., Mathammal, R.: Structural elucidation and physicochemical properties of an organic NLO crystal: 4-nitrotoluene-2-sulphonic acid dihydrate. J. Mol. Struct. **1155**, 598–609 (2018). https://doi.org/10.1016/j.molstruc.2017.11.048

Sathyavathi, R., Krishna, K.M., Rao, S.V., Venugopal, S.V., Rao, D.N.: Biosynthesis of silver nanoparticles using *Coriandrum sativum* leaf extract and their application in nonlinear optics. Adv. Sci. Lett. **3**(2), 138–143 (2010). https://doi.org/10.1166/asl.2010.1099

Sindhusha, S., Padma, C.M., Thayanithi, V.: Experimental and theoretical investigations of organic creatininium 2-chloroacetate nonlinear optical single crystal. J. Mater. Sci. Mater. Electron. **32**, 6498–6510 (2021). https://doi.org/10.1007/s10854-021-05367-x

Singla, N., Tripathi, A., Rana, M., Goswami, S.K., Pathak, A., Chowdhury, P.: Turn on/off" proton transfer based fluorescent sensor for selective detection of environmentally hazardous metal ions (Zn2+, Pb2+) in aqueous media. J. Lumin. **165**, 46–55 (2015). https://doi.org/10.1016/j.jlumin.2015.04.007

Song, Y.Z., Wang, J., Li, M.T., et al.: Electrochemical catalytic reduction of p-nitrotoluene on the surface of α-Ag_2S crystal. Russ. J. Phys. Chem. **96**, 899–906 (2022). https://doi.org/10.1134/S003602442204029X

Sukma, H.A., Hendra, H., Steven, K.Y.: Investigation of the chemical and optical properties of halogen-substituted N-methyl-4-piperidone curcumin analogs by density functional theory calculations. Spectrochim. Acta A Mol. Biomol. Spectrosc. **1233**, 117152 (2019). https://doi.org/10.1016/j.saa.2019.117152

Weeraratna, C., Amarasinghe, C., Lu, W., Ahmed, M.: A direct probe of the hydrogen bond network in aqueous glycerol aerosols. J. Phys. Chem. Lett. **12**(23), 5503–5511 (2021). https://doi.org/10.1021/acs.jpclett.1c01383

Wen, L., Zhou, L., Zhang, B., Bingguang, M., Meng, X., Qu, H., Hua, D., Li, D.: Multifunctional amino-decorated metal–organic frameworks: nonlinear-optic, ferroelectric, fluorescence sensing and photocatalytic properties. J. Mater. Chem. **22**(42), 22603 (2012). https://doi.org/10.1039/c2jm34349e

Yadav, P., Rana, M., Chowdhury, P.: DFT and MD simulation investigation of favipiravir as an emerging antiviral option against viral protease (3CLpro) of SARS-CoV-2. J. Mol. Struct. **1246**, 131253 (2021). https://doi.org/10.1016/j.molstruc.2021.131253

Yakovenko, A.A., Antipin, M.Y., Timofeeva, T.V.: Molecular and crystal structure of low melting nitrotoluene isomers. Cryst. Growth Des. **9**(1), 57–65 (2009). https://doi.org/10.1021/cg800659f

Yanxin, Y., Yulin, H., Pan, L., Hui, Z., Qiuying, Z., Jialiang, L., Linghan, X., Xibin, W., Yuhui, A., Ming, L.: Mild and in situ photo-crosslinking of anthracene-functionalized poly (aryl ether ketone) for enhancing temporal stability of organic NLO materials. J. Mater. Sci. **56**, 5910–5923 (2021). https://doi.org/10.1007/s10853-020-05594-3

Yanzhu, L., Qingyan, S., Hongbo, Z., Hongya, G., Dongping, L., Yongxiu, L.: One-dimensional Europium-coordination polymer as luminescent sensor for highly selective and sensitive detection of 2,4,6-trinitrophenol. Spectrochim. Acta A Mol. Biomol. Spectrosc. **264**, 120303 (2022). https://doi.org/10.1016/j.saa.2021.120303

Zaini, M.F., Arshad, S., Thanigaimani, K., Khalib, N.C., Zainuri, D.A., Abdullah, M., Razak, I.A.: New halogenated chalcones: synthesis, crystal structure, spectroscopic and theoretical analyses for third-order nonlinear optical properties. J. Mol. Struct. **1195**, 606–619 (2019). https://doi.org/10.1016/j.molstruc.2019.05.122